Design of a Robotic Jet Thruster for an Aquatic Micro Air Vehicle

Robert Siddall, Mathieu de Launay and Mirko Kovač
Imperial College London
Aerial Robotics Laboratory
London, United Kingdom
r.siddall13@imperial.ac.uk, m.kovac@imperial.ac.uk

***Abstract*— Currently, no robot exists that is capable of both underwater locomotion and flight. This is principally because of the difficulty a neutrally buoyant vehicle has in achieving take-off speed from water. The use of high power density jet propulsion would allow short, impulsive take-offs by Micro Air Vehicles. In this paper, we propose the design of a high power water jet based propulsion system for an Aquatic Micro Air Vehicle (AquaMAV), designed to produce up to 37N of thrust, with a mass of 33 grams. When launched from the ground, the mechanism would leap up to 15m high. We present first tests and discuss planned design optimisations with the aim of creating an integrated AquaMAV.**

I. Introduction

Locomotion in unstructured terrain is one of the most significant challenges to robots operating in a realistic environment. The problem becomes even more complicated in the presence of water. Whilst many amphibious robots exist, these robots are not able to cross large, sheer obstacles, and can only exit the water on a gentle incline. Floatplane-style Micro Aerial Vehicles (MAVs) are also equally inhibited by the presence of obstacles in the water, requiring a large, clear area to take off, preventing them from entering confined spaces [1].

An Aquatic Micro Aerial Vehicle (AquaMAV) capable of leaping into the air from the water would find use in disaster relief [2] and oceanography [3], [4], particularly in areas such as flooded collapsed buildings, or rocky, littoral ecosystems where obstacles impede the free movement of conventional aquatic vehicles, and prevent close observation by purely aerial robots. Several unmanned seaplanes are currently in operation [5], and studies have shown the potential of an aerial-aquatic robot that is propelled by adaptable flapping wings [6], or able to plunge dive into water [7]. However, to the best of the author's knowledge, no aerial-aquatic vehicle has been realised to date.

Use of high power density propulsion would allow a vehicle to take off from a confined space of water (figure 1). This would mean that an AquaMAV could dive into an isolated area of water, where it could collect water samples and return underwater video footage. The vehicle could then perform a short take-off, and return to its launch site to submit collected samples and data for analysis. This would enable a fast, targeted response to emergency scenarios such as a stricken ship or a tsunami event, that could not be matched by conventional aquatic robots.

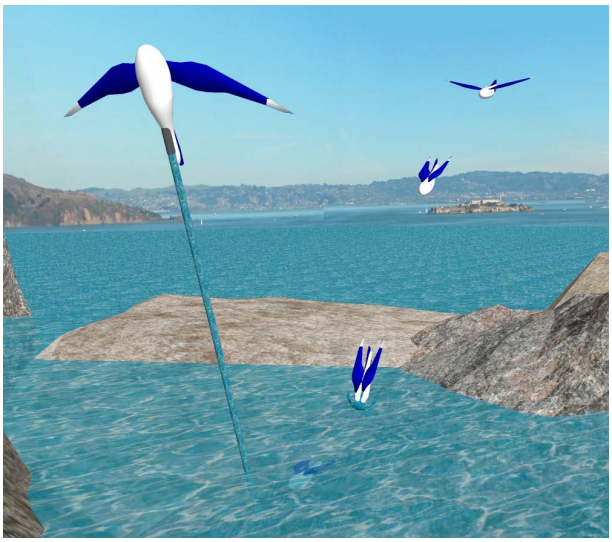

Fig. 1. A plunge diving AquaMAV can enter confined spaces of water for data collection, before retaking flight with a high power impulsive take-off

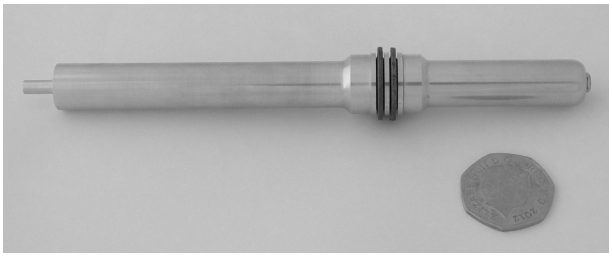

Fig. 2. This fabricated aluminium robotic jet is designed to achieve vertical launch heights over 100 times its size.

Fig. 3. Jet propulsion is used as a means of take-off by Flying Squid, to initiate extended jumpgliding leaps. *Credit: Bob and Deb Hulse*

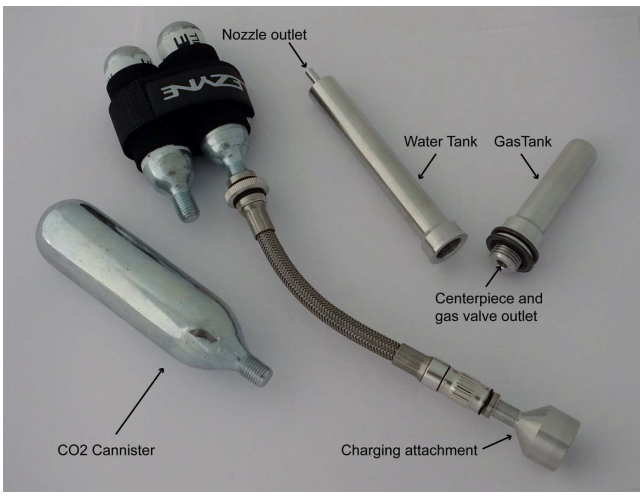

Fig. 4. The robotic jet has separated gas and water tanks, which allows an AquaMAV to collect propellant water during a dive, rather than carry it. Small, portable CO_2 cannisters can be used for rapid recharging.

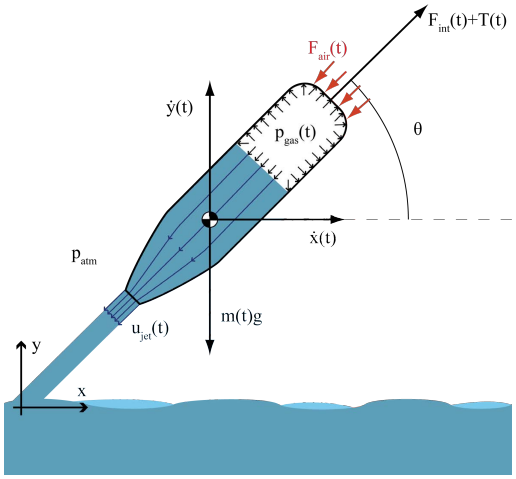

Fig. 5. Jet propulsion principle. Compressed gas expels water through a nozzle, propelling the vehicle.

In nature, a wide variety of animals are capable of crossing aquatic obstacles with ease by leaping from the water surface [8]. This can be achieved by swimming at high speed through the surface (flying fish, salmon), foot propelled surface jumping (mole crickets, basilisk lizards) or by flying appendages (seabirds). Uniquely, several species of squid are able to initiate gliding leaps by expelling a pressurised jet of water [9] (figure 3).

This jet propelled launch is uniquely applicable to short take-offs by AquaMAVs. Unlike swimming leaps or foot propelled jumps, a jet continues to produce thrust in both air and water. This allows a vehicle to lift free of the water and continue accelerate when airborne, where drag is dramatically reduced compared to locomotion in water [8]. Unlike foot propelled jumping, jet propelled devices are also not sensitive the the rigidity of their launch area, and can jump from soft surfaces like leaves, mud or snow.

In this paper we present a 33.5 gram miniature jumping robot powered by compressed air, which has a predicted vertical jump height of over 15m, or 100 times its length. This robot uses a shape memory alloy actuated valve to control the release of stored carbon dioxide (CO_2), which is used to expel propellant water mass.

In the following sections, we introduce the physical principles behind water jet propulsion, and detail the key design features of a jet-propelled jumping robot, including selection of its overall geometry by simulation. Successful actuation of the fabricated device is then demonstrated.

II. Design

Here we detail the key objectives in the vehicle design process, and the underlying theory behind water jet propulsion. We then present the implemented design solutions and the first prototype that resulted.

A. Objectives

The robot is to form a critical component of a plunge diving AquaMAV, producing the thrust required to leap from the water surface after diving. Because it is intended for use in sustained flight, the device must be as lightweight as possible. The planned AquaMAV will weigh approximately 100 grams, and a maximum mass budget of 50 grams has been allocated for the water launch system. After a dive, the device will be actuated on the water surface and must propel the AquaMAV to a velocity sufficient for sustained flight. This means that the actuation of the device must be entirely self contained, and thrust production must not be sensitive to the variations in attitude due to the motion of the water surface.

Water jet propulsion is often used in science education in the form of simple plastic water rockets [10]. However, the water rockets common in schools and amongst hobbyists are generally launched vertically, and use an off-board launchpad to both contain the pressure and actuate the rocket. These devices also contain air and water free to mix within a single chamber, relying on gravity and the rocket's acceleration to separate the two. If these rockets are at too shallow an angle the compressed gas can be expelled whilst water remains inside, resulting in little thrust and unexpelled mass.

To launch an AquaMAV from the water surface, the device actuation must be entirely self contained and insensitive to variations in attitude. In order to be able discharge the device effectively at any angle or during 'sloshing motion', air and water must be kept separately. This also minimises device weight, as it allows water to be collected *in situ* at launch, rather than carried.

In order to create a powerful, but practical and portable device, it was decided to design a vessel that could be charged using commonly available high pressure CO_2 cannisters, which hold gas at 60bar (figure 4). CO_2 is used because it is more compressible than air, and so stores more energy for

a given pressure and volume. The principal design challenge was then to maximise the launch height of the device, based on the use of 60 bar gas as an energy source, whilst staying within a mass budget of 50 grams.

B. Water Jet Propulsion Theory

The thrust produced by an expelled jet of mass is given by:

$$T = \dot{m} u_{jet} \tag{1}$$

If a gas is used as the propellant mass, its low density means that thrust production is negligible without very high exit velocities, and for efficient propulsion, a heavier propellant must be used. For an AquaMAV, water is a propellant that can easily be collected before launch. Because of this, the presented robot has been designed to use water as its propellant mass, driven by the expansion of compressed gas.

The incompressibility of water means the expelled jet will be at atmospheric pressure, and the gas expansion rate will equal the water outflow (2). Upstream of the jet the flow can be treated as quasi-1D by assuming uniform flow across the jet section, with purely axial fluid velocity. By mass continuity, the local velocity is then a function of cross-sectional area. The unsteady form of Bernoulli's equation (3) can be recovered from Euler's equation by integrating from the air-water interface to the nozzle exit (figure 5) [11]. Total pressure along a streamline between these two points is equal to the instantaneous gas pressure, multiplied by a resistance coefficient, η, that represents the losses due to viscosity as a pressure drop.

$$u_{jet} = \frac{\dot{V}_{air}}{A_{exit}} \tag{2}$$

$$\int_1^2 \frac{\partial u}{\partial t} ds + \frac{\eta p_{gas}}{\rho_w} + \frac{1}{2}(u_1^2 - u_2^2) = 0 \tag{3}$$

Where u is the water velocity, p_0 is the initial gas pressure, V is the gas volume, A_{exit} is the nozzle exit area and ρ_w is the density of water. The gas expansion takes place over a very short time period, which means that heat transfer can be neglected [10], and the expansion process can be treated as adiabatic. The instantaneous gas pressure can then be given by the isentropic gas relation:

$$p_{gas} = p_0 \left(V_0 / V_{air}\right)^{\gamma} \tag{4}$$

Combining equations 2-4 leads to a non-linear second order differential equation in $V(t)$. The variation of V with time is then be obtained by numerical integration using a Runge-Kutta scheme, which in turn allows thrusts and launch trajectories to be computed. During launch, an additional force term, $F_{int}(t)$ is included to account for the force experienced by the vessel due to the internal acceleration of fluid mass [11].

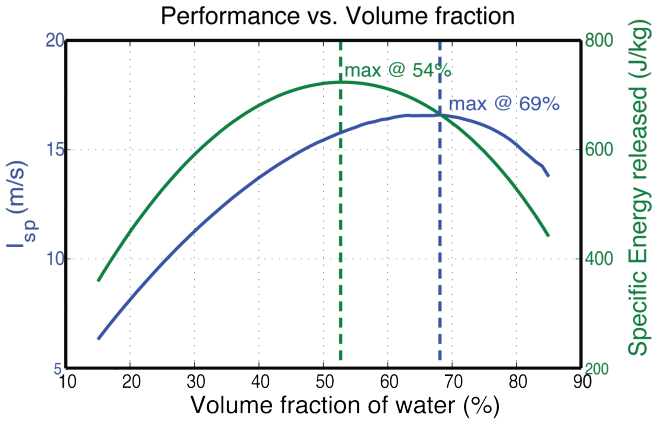

Fig. 6. Specific impulse can be maximised for a given geometry by varying the volume fraction of water. Maximising energy density does not yield maximum performance. This plot shows the simulation results for the fabricated geometry.

$$F_{int} = -\int \rho_w \frac{\partial u}{\partial t} dV_{water} \tag{5}$$

For a given pressure, the volume of air before launch determines the total energy stored. Once the stored water has been exepelled, further gas expansion produces negligible thrust, but if too little gas is stored, there is insufficient energy to expel all the water at significant speed. There then exists an optimum ratio of air to water. For a given volume, pressure and vessel mass, the ratio that gives the maximum specific energy release can be calculated analytically. However, because much of this energy is tranferred as kinetic energy to the expelled waterm maximising energy density will not yield the maximum launch height. To obtain this optimum, the system specific impulse (I_{sp}) is numerically computed and used as an objective, maximising the momentum imparted to the thruster (figure 7B).

$$I_{sp} = \int T + F_{int} dt / m_{total} \tag{6}$$

C. Pressure Vessel Design

The vessel was designed to the European standard for high pressure vessels (EN 13445) [12]. Aluminium was used for the vessel body, principally for the ease with which it could be machined, which reduced the complexity and time associated with production of the device. For aluminium alloy 6082, the standard dictates a design stress of 96MPa, based on a yield stress of 290MPa. However, laboratory health and safety concerns meant that this was further decreased to 48MPa, an additional safety facor of 2. This means that the final mass of the vessel is approximately double the minimum that it could feasibly be, whilst still meeting international standards.

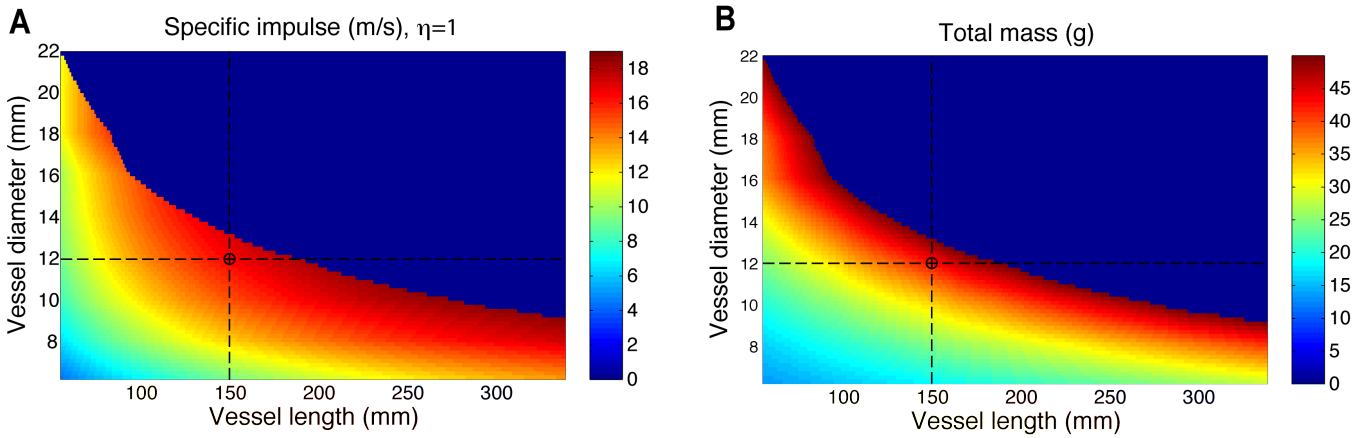

Fig. 7. The design landscape for a <50g aluminium thruster, with the fabricated geometry indicated: (A) Variation of I_{sp} with geometry, for a lossless jet. (B) Variation of mass with geometry.

D. Design Domain

To select the vessel geometry, the design domain for the pressure vessel was characterised by numerical simulation across a range of internal vessel geometries (figure 7). At each given internal diameter and total length, the mass of the vessel is computed based on the specified design stresses, and the thrust is simulated for a range of air:water ratios to obtain the optimum mix for that geometry. The design domain was then mapped for the range in which the total vessel mass (including propellant water) is less than 50 grams (figure 7B). The computed vessel mass also accounts for the masses of the gas release valve and actuation system, which does not scale with vessel size, and this results in non linearities.

The specific impulse of the device can be seen to broadly increase with increasing volume, but as length is reduced, increasing the vessel diameter delivers decreasing returns in performance (figure 7A). The first fabricated vessel has 1.1mm thick walls and an inner diameter of 12mm. The air tank stores 4.8ml of air, while the water tank stores 10.7ml of water, to give the optimum mix ratio of 69%. Performance increases could have been achieved by increasing the vessel length (figure 7A), but this was not possible due to machining limitiations. Future thruster iterations will move closer the the maximal performance.

E. Prototype

The initially produced design consists of an air and water tank, both with sealed screw connections to a connecting centrepiece. For simplicity, the first iteration of this centrepiece contains a common Schrader^{TM}valve core. This valve is then actuated by Flexinol^{TM}NiTi shape memory wires to release the gas on command. The vessel is constructed almost entirely from aluminium using CNC machines, and has a modular construction, with the centrepiece and its valve actuation system entirely self contained, so that it can be easily removed.

It was decided that in order for the device to be functional, the pressure release system must also be reusable, which precluded the use of 'single shot' systems such as a bursting diaphragm. For initial tests of the release system concept, an off the shelf Schrader poppet valve has been used. This valve has a small opening, and will significantly impede the expulsion of gas. However, it can be easily adapted to be actuated with shape memory wires, and is suitable as a proof of concept while a larger bore valve is produced, which minimises compressible gas flow losses.

The valve is opened by moving the valve stem a vertical distance of 1.6mm. When under 60 bar of internal pressure, the force required to open the valve is 42N, (37N of pressure force, 5N from the valve internal spring). These high force, short stroke actuation requirements are well suited to the use of Nitinol shape memory alloy (SMA) wire, and a high pressure valve actuation system was designed, employing 0.51mm Flexinol wires. These wires can produce repeatable contraction forces of up to 35.6N upon heating to 90^{o}C [13]. Heating is achieved by passing a 5A, 0.5 second current pulse through the wire.

After contraction, the wires must be stretched to their original length. This requires a stress of 69MPa, which corresponds to a minimum total force of 23.2N in addition to the internal spring. To achieve this with minimal mass and volume, a pair of buckling spring steel wires with pinned ends are used (figure 8A). The wires are treated as elastic beams, and the large deformation elastica problem is solved analytically using elliptical integrals [14]. To achieve the required average force over the valve stroke, with the wire length constrained to be below 40mm, the wire diameter was set to 0.6mm, with a length of 34mm, giving an average force of 11.6N per wire.

The valve actuation is contained within the pressurised gas tank, so that it does not impede attachment to a CO_2 canister for charging. To provide sufficient stroke and force, two 34mm long Flexinol wires are attached to the valve stem. The wires pull against a frame formed by two carbon fibre rods and a steel tube, mounted into the centrepiece. The steel tube provides an electrical connection to the centrepiece, as

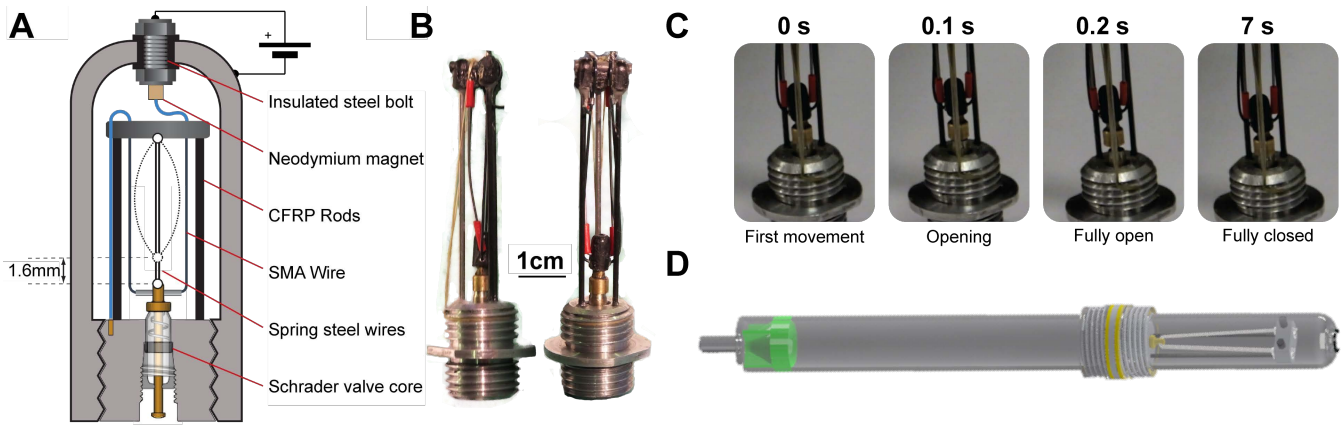

Fig. 8. (A) Schematic of valve opening mechanism, with the vessel body forming a negative earth. (B) Fabricated valve actuator. (C) Valve actuation times under a 5A, 0.5s current pulse. (D) Transparent CAD rendering of the fabricated jet, showing removeable plastic nozzle and valve actuation system.

it was difficult to achieve a good connection through the carbon rods (figure 8B).

To provide an electrical conduit through the pressurised container, the entire vessel was used as a negative earth and an insulated steel bolt was fastened through the rear of the tank (figure 8A). This allows a complete circuit for wire actuation to be formed, without compromising the gas tank seal. To complete the circuit, a neodymium magnet wired to one end of the Flexinol wire attaches to the steel bolt when the valve assembly is inserted. The other end of the SMA wire is connected to the centrepiece through the steel tube support, allowing the valve assembly to be readily removed.

Fianlly, design of the water nozzle is critical to the final design performance. Using a simple orifice plate as a nozzle, while minimising weight, would result in a discharge coefficient of around 0.65 [15] (corresponding to $\eta = C^2_{disch} = 0.43$). However, the gradual contractions often used in flowmeters and water jet cutters can reduce flow resistance to near unity. Initially, a nozzle with a 30^o cone angle has been used, connected by tangential arcs to the straight inlet and outlet sections. To implement this nozzle into the aluminium vessel, the water tank was produced with a flat end and simple orifice contraction. A nozzle was then 3D printed with the desired tangential geometry and inserted into the aluminium water tank (figure 8D). This arrangement reduces manufacturing complexity, and allows easy modification of the nozzle geometry later.

III. Initial Results

With no losses, the fabricated design is predicted to produce a maximum thrust force of 37N, with an I_{sp} of 16.5m/s (figure 9A). If the device is treated as a projectile with a conservative drag coefficient of 1.5, this would result in a peak height of over11m from a 60^o launch (figure 9B).

Once fabricated, the valve actuation system was first tested outside of the vessel, connected to a constant current source, and was able to perform repeated actuations without loss in performance. High speed (480fps) video showed that the time taken for the valve to open from the first movement of the wires is 200ms (figure 8C). The negative earth electrical conduit into the tank also functioned as expected, and the device was able to discharge the contained gas on command. The device was then mounted to a load cell, and the thrust produced was measured.

TABLE I
WEIGHT BUDGET

Part	material	weight [g]
Water Tank	Aluminium	14.97
Gas Tank	Aluminium	9.80
Centrepiece and Valve	Aluminium and Steel	5.87
Plastic nozzle insert	Connex ABS	1.87
Shape Memory Wire	Flexinol (NiTi)	0.16
SMA Wire mounts	Aluminium + Steel	0.80
Total mass prototype		**33.47**

The measured thrust profile show significant losses in the discharge system, reducing the maximum thrust by a factor of 8. It can be seen that the peak thrust is delayed, and this is expected to be due to the valve opening time, which is much larger than the time taken for discharge (figure 9C). This has lead to high losses, in addition to those resulting from the valve's small size. The result of these losses is a specific impulse reduced by 25%, corresponding to an averaged loss coefficient of η =0.52 (figure 9D). However, the reduction in maximum thrust is more significant to the design, as a vehicle taking off from water will initially need high power density to overcome surface water drag [1].

IV. Discussion

Some of the gas losses in the actuation system can be addressed by increasing the actuation speed of the wire. Increased heating rates will require shorter current pulses with higher currents, which would not be achieveable with

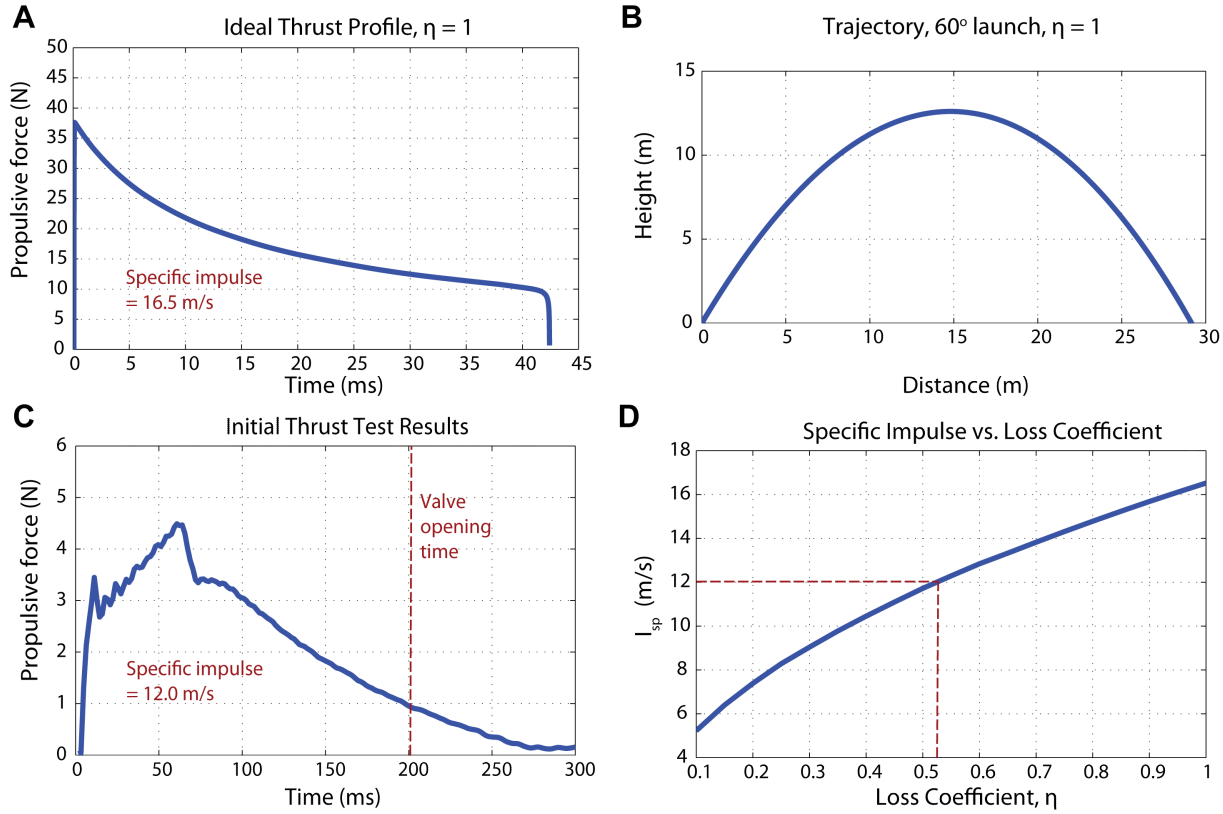

Fig. 9. Simulated and experimental performance of the fabricated jet: (A) Predicted thrust profile for the jet with zero losses. (B) Predicted trajectory from a 60^o launch of the jet with zero losses. (C) Thrust profile of a proof-of-concept jet test. The gas is discharged faster the an the valve can open, resulting in high losses. (D) The effect of losses on the jet's specific impulse.

batteries. However, the shape memory wire used has a low resistance of 0.3Ω which would allow very high currents to be generated from low voltage supercapacitors with minimal mass. However, due to the high opening loads, increased wire contraction rates will reduce the device longevity.

The remaining losses will come from viscous effects in both the gas valve flow and the water nozzle flow. The compressed gas is flowing through an orifice, which will entail large losses. This will be addressed both by designing a new large valve and by modifying the centrepiece geometry around the inlet to minimise losses. Viscous losses are given only a rudimentary representation in the design model, and in order to achieve a truly optimised design, the effects of scale on the device efficiency will need to be characterised. Future work will combine empirical loss estimates with CFD analysis in order implement discharge loss into the design domain model, and minimise its effects. The current prototype allows the water nozzle design to be easily removed and changed (section II-E), which will allow performance to be experimentally investigated.

At the end of the water expulsion, the velocity of the air-water interface increases rapidly as it passes through the nozzle contraction. At this point, fluid wall shear and 'plughole' vortical instabilites cause the interface to become non-planar, and allow air to escape before all water has been expelled. The effect of this mixing can be observed in the tapering thrust profile in figure 9C compared to the abrupt end predicted by theory (figure 9A). The effect of this on the jet performance, and the means of its suppression will be characterised by thrust tests accompanied by high speed video. A transparent water nozzle is also being fabricated, to be used in low pressure tests and allow viewing of the internal flow.

While performance can be readily increased, the fabricated system has demonstrated the viability of the design. The valve actuation system has been intentionally designed to lend itself to modification of the final design geometry, and owing to the modular construction, the air and gas tanks can be easily refabricated with different dimensions. The robot is also a functional, lightwieght, internally actuated compressed gas storage system, and such a system system would have many different potential applications outside of propulsion, such as inflatable structure deployment.

The energy density of a compressed gas water jet broadly scales with the specific strength of the vessel material. The aluminium used for this device has a specific ultimate strength of 107kNm/kg. Materials such as titanium and carbon fibre have much higher strength to weight ratios (300kNm/kg and 2300kNm/kg respectively), and their use could yield significant reductions in mass. However, non-

linearities in vessel weight scaling will again occur, due to minimum produceable thicknesses and sealing requirements, which must also be factored into the design.

V. Conclusions and Future Work

In this paper we have presented the design and fabrication of a novel water jet propelled robot. The modular design of this device means that it can be readily modified, and a theoretical model has been developed which will allow water jet thrusters to be optimised depending on the desired overall size and performance.

The valve used in the robot has been used for convenience as a proof of concept, and results in high losses. A larger replacement valve is being fabricated, using the same system of buckling bars and nitinol for actuation. This will greatly reduce the losses in the gas release system. The final design will incorporate detailed quantification of nozzle losses into the design domain model, so that maximal performance is achieved.

The final robot will be used as an experimental platform for the investigation of aquatic jumpgliding, and will be fitted with appropriate lifting surfaces. This will allow the mechanics of short take-off from water to be characterised for miniature robots, and provide a pathway for the development of the first Aquatic Micro Aerial Vehicle.

VI. Acknowledgements

The authors would like to acknowledge the technical staff in the Imperial College Aeronautics department, in particular Roland Hutchins, Andrew Wallace and Mark Grant, whose help was indispensible during the project. Thanks also go to Yi Wei Tan for his work on initial experiments. This project is being funded by the UK Engineering and Physical Sciences Research Council.

References

[1] R. Siddall and M. Kovač, "Launching the AquaMAV: Bioinspired design for aerial-aquatic robotic platforms," *Bioinspiration and Biomimetics, in press*, 2014.

[2] S. Kawatsuma, M. Fukushima, and T. Okada, "Emergency response by robots to fukushima-daiichi accident: summary and lessons learned," *Industrial Robot: An International Journal*, vol. 39, no. 5, pp. 428–435, 2012.

[3] P. Stevenson, S. McPhail, M. Tsimplis, and E. Higgins, "Air launched platforms-a new approach for underwater vehicles," in *OCEANS 2009-EUROPE*. IEEE, 2009, pp. 1–8.

[4] F. Shkurti, A. Xu, M. Meghjani, J. C. Gamboa Higuera, Y. Girdhar, P. Giguere, B. B. Dey, J. Li, A. Kalmbach, C. Prahacs, *et al.*, "Multi-domain monitoring of marine environments using a heterogeneous robot team," in *Intelligent Robots and Systems (IROS), 2012 IEEE/RSJ International Conference on*. IEEE, 2012, pp. 1747–1753.

[5] G. Meadows, E. Atkins, P. Washabaugh, L. Meadows, L. Bernal, B. Gilchrist, D. Smith, H. VanSumeren, D. Macy, R. Eubank, *et al.*, "The flying fish persistent ocean surveillance platform," in *AIAA Unmanned Unlimited Conference*, 2009.

[6] R. J. Lock, R. Vaidyanathan, S. C. Burgess, and J. Loveless, "Development of a biologically inspired multi-modal wing model for aerial-aquatic robotic vehicles through empirical and numerical modelling of the common guillemot, uria aalge," *Bioinspiration & Biomimetics*, vol. 5, no. 4, p. 046001, 2010.

[7] J. Liang, X. Yang, T. Wang, G. Yao, and W. Zhao, "Design and experiment of a bionic gannet for plunge-diving," *Journal of Bionic Engineering*, vol. 10, no. 3, pp. 282–291, 2013.

[8] J. Rayner, "Pleuston: animals which move in water and air," *Endeavour*, vol. 10, no. 2, pp. 58–64, 1986.

[9] R. ODor, J. Stewart, W. Gilly, J. Payne, T. Cerveira Borges, and T. Thys, "Squid rocket science: how squid launch into air," *Deep Sea Research Part II: Topical Studies in Oceanography*, 2012.

[10] J. M. Prusa, "Hydrodynamics of a water rocket," *SIAM review*, vol. 42, no. 4, pp. 719–726, 2000.

[11] C. J. Gommes, "A more thorough analysis of water rockets: Moist adiabats, transient flows, and inertial forces in a soda bottle," *American Journal of Physics*, vol. 78, p. 236, 2010.

[12] E. DIN, "13445-3,"," *Unfired Pressure Vessels–Part*, vol. 3, 2005.

[13] J. M. Conrad and J. W. Mills, "Appendix d: Technical characteristics of flexinol actuator wires," *Dynalloy, Inc.), Stiquito: Advanced Experiments with a Simple and Inexpensive Robot*, pp. 301–309, 1997.

[14] C. Wang, *Applied elasticity*. McGraw-Hill, 1953. [Online]. Available: http://books.google.co.uk/books?id=P_tQAAAAMAAJ

[15] F. M. White, *Fluid Mechanics (Sie)*. McGraw-Hill Education (India) Pvt Limited, 2011. [Online]. Available: http://books.google.co.uk/books?id=zxsGt2OvTo0C